Advances in Water Resources 151 (2021) 103888

Contents lists available at ScienceDirect

Advances in Water Resources

journal homepage: www.elsevier.com/locate/advwatres

Insight into particle detachment in clogging of porous media; a pore scale study using lattice Boltzmann method

Amin Parvan[a], Saeed Jafari[a,*], Mohammad Rahnama[a], Saeid Norouzi-Apourvari[b], Amir Raoof[c]

[a] Department of Mechanical Engineering, ShahidBahonar University of Kerman, Kerman, Iran
[b] Department of Petroleum Engineering, ShahidBahonar University of Kerman, Kerman, Iran
[c] Department of Earth Sciences, Utrecht University, Utrecht, the Netherlands

ARTICLE INFO

Keywords:
Porous media
Pore scale
Detachment process
Lattice boltzmann method
Attachment process
Fine particles clogging

ABSTRACT

Clogging of porous media is controlled by attachment of particles and their subsequent detachment. In this study, we explore particle transport at the pore scale by considering attachment and detachment processes. We use pore structures of three samples which have similar topological properties but different initial porosities. The main focus is on particle detachment, after they are attached to the solid grain boundaries, and to explore how particle detachment affects hydraulic properties and clogging of porous media. A new approach was proposed by combining the lattice Boltzmann method with a Lagrangian method to simulate fluid flow and particle transport, respectively. Comparisons between several simulations, with and without detachment, were used to evaluate the impact of particle detachment on fluid flow velocity distributions. The coefficients of Carman-Kozeny relation were used to relate porosity changes of each sample to its permeability alterations. Additionally, the influence of the initial porosity of the sample and flow velocity on the detachment process was analysed. The results show that compared to the impact of flow velocity, the initial porosity of the media has a greater influence on controlling the rate of detachment and change of pore structures.

1. Introduction

Understanding attachment and detachment of fine particles in porous media is critical in several applications including chemical (Stewart and Buriak, 2000) environmental ((Abdul Mujeebu et al., 2009); Raoof and Hassanizadeh 2010, Raoof et al., 2010), and petroleum technologies, oil exploitation (Parazzo et al., 2018), industrial filtering (Netter and Conti, 2016), groundwater utilization (Chequer et al., 2019;Wang et al., 2020), grouting engineering (Zhou et al., 2018) and industrial waste disposal (Tong et al., 2019). Several approaches including experimental (Bergendahl and Grasso, 2000; Silliman et al., 2001; (Haque et al., 2017), Chu et al., 2019), computational (Raoof et al., 2013; Klimenko and Maryshev, 2019; (Benioug et al., 2017; Gaebler and Eberl, 2018), Yoon et al. 2015; and mathematical (Bedrikovetsky et al., 2011, (Bedrikovetsky et al., 2012), Bergendahl and Grasso, 2000; Schulz and Knabner, 2016) methods have been developed, focusing on particle transport, attachment, and detachment of colloids in porous media. Attachment of particle at the solid grains alters topology and geometry of the pore structure and varies the fluid flow regime. At the same time, attachment of particles increases the hydrodynamic shear next to the grain surfaces which may cause detachment of the deposited particles.(Coronado and Diaz-Viera, 2016) studied permeability loss due to fine migration and clogging using three experiments. Based on the study of Bedrikovetsky et al. (2011), they applied an extended mathematical model to simulate permeability impairment. Endo Kokubun et al. (2019) explored the effect of hydrodynamic forces on accumulation of particles in water-saturated porous media. Their numerical results showed significant accumulation of particles in both low and high-velocity regions. They reported that during particle transport in homogeneous media, particles are significantly accumulated in low-velocity regions, however, the ultimate porous media clogging is occurred at high velocity regions. In addition to particle attachment and retention, detachment of fine particles can play a significant role in the clogging behaviour of porous media.

Several studies have included particle detachment process to obtain effective parameters for adsorptive transport (Tufenkji, 2007; Kapellos, et al., 2007; Han et al., 2019; (Zhang et al., 2019)). Zheng et al. (2014) used a combined experimental-mathematical analysis, and found that detachment does not necessarily occur under lower Darcy velocities and there exist a significant relation between the attachment/detachment parameters and flow velocity. Cui et al. (2017) evaluated the influence of flow velocity and its direction on detachment process using experimental observations. Quartz powder with sizes of 18 and 41 μm were used as colloids and quartz sand was used as porous media. They observed that both parameters influence the detachment rate of the deposited particles, however, the magnitude of fluid velocity showed a larger impact on the detachment rate. (Huang et al., 2017) in-

* Corresponding author.
E-mail address: jafari@uk.ac.ir (S. Jafari).

https://doi.org/10.1016/j.advwatres.2021.103888
Received 7 November 2020; Received in revised form 5 February 2021; Accepted 8 March 2021
Available online 14 March 2021

Nomenclature

f_α	Boltzmann distribution function
c_α	Velocity vector in α-direction
τ	Hydrodynamic relaxation time
f_α^{eq}	Equilibrium distribution function
C	Lattice sound speed (m/s)
Δx	Lattice length
Δt	Lattice time
ω_α	Weight coefficient for the α-direction
C_s	Sound speed (m/s)
υ	Kinematic viscosity(m^2/s)
ρ	Fluid density (kg/m^3)
$\mathbf{u}$	Fluid velocity (m/s)
m	Mass of particle (kg)
v	Particle velocity (m/s)
F_D	Hydrodynamic drag force
μ	Dynamic viscosity (Pa.s)
a_c	Particle radius (m)
$\boldsymbol{\sigma}$	Shear stress (Pa)
$\boldsymbol{\sigma_{cr}}$	Critical shear stress(Pa)
$\boldsymbol{F_N}$	Adhesive force (N)
$\boldsymbol{c_f}$	Friction coefficient
k_t	Particle stickiness to surface (m)
C_p	Particle mass concentration
α	Empirical constant
H	Hamaker coefficient
l	Separation distance between the particle surfaces in filter cake (m)
$N_{M_{cr}}$	Critical mobility number
$N_{Re_{cr}}$	Critical Reynolds number
v_{cr}	Critical shear velocity (m/s)
γ_s	Specific weight of particle
Re	Reynolds number
K	Permeability(m^2)
K_0	Initial permeability(m^2)
ϕ	Porosity
ϕ_0	Initial porosity
i	Horizontal nodes counter
j	Vertical nodes counter
nx	The number of lattice nodes in horizontal direction
ny	The number of lattice nodes in vertical direction
φ_s	Sphericity
$\underline{\tau}$	Stress tensor
σ_t	Standard deviation
$\bar{\tau}$	Mean stress
τ^*	Normalized shear stress

vestigated the role of flow conditions, fine sizes and fracture aperture on particles detachment during dewatering process. A mathematical model was developed to describe single particle detachment mechanism. They found a critical pressure gradient under which a massive amount of fine detachment occurred. Their results showed that, with increasing the size of fine particles, the pressure gradient required for fine detachment initially decreased to a minimum value (called critical gradient pressure) and subsequentlyincreased to a larger value. During the attachment and detachment of fine particles permeability alterations occur due to porosity variation and change of pore structures.

The complex nature of porous media have caused challenges in developing relationships among permeability, porosity, grain size and fine sizes (Hommel et al., 2018). Several modelshave been developed to predict the permeability reduction due to particles retention including experimental (Verma and Pruess, 1988; Civan, 2001; Thullner, 2010; Bacci et al., 2011) and numerical (Zhang et al., 2015; Ju et al., 2017; Joodat et al., 2018) approaches. While some studies have applied a more realistic and complex pore structures (Xiao and Yin, 2016; Rabbani et al., 2018), many others were limited to simpler grain geometries like cylindrical shapes (Yazdchi et al., 2011; Endo Kokubun et al., 2019). Porous media with identical porosity values often have different topologies (i.e., the way that pore structures with different sizes are interconnected). This difference can significantly affect the relationship between porosity and permeability of porous media which even have similar porosities. Lima et al. (2020) showed that samples with higher pore connectivities (i.e., larger pore coordination numbers) provide much larger permeabilities compared to samples with similar porosities but with a less number of connected pores. Deo et al. (2010), in an experimental-modelling study, investigated the permeability reduction in concrete samplesby retention of fine particles and pore clogging. They used fine and coarse concrete samples as the matrix materials and observed a substantial permeability reduction when an incremental amount of finer sand was added to the porous concrete mixtures. Based on their observations, they proposed a ratio of pore size to particle size under which permeability reduction is maximum and its reduction would not have a significant trend for coarser sands. Sato et al. (2013) investigated the effect of trapped particles on permeability reduction using an image of real sand grains and applying Lattice Boltzmann Method (LBM) to simulate fluid flow. They used volume fraction and specific surface areas of both grains and the clogging particles to define a relation for permeability alteration. They found that the reduction in permeability could not only be attributed to changes in volume fraction of fine particles to the pore volume, but also to the size distribution of fine particles. According to their results, when medium porosity is more or lessconstant along the sample, the order of magnitude of the resulting permeabilities is identical to porosity values, whether the fine particles are fixed at random positions or they are trapped within the narrow pore throats. Montessori et al. (2015) and (Montessori et al., 2016) employed lattice Boltzmann method to simulate strongly non-equilibrium flows in porous media and reactive flow related to nano porous materials. Their results showed that non-equilibrium effects increase the reactivity of the porous sample and provided quantitative assessment of the reactivity using the thickness of the reactive layer inside a nano-porous catalytic sample.

Ahfir et al. (2016) investigated the influence of porous medium grain size and fine particle sizes on clogging and found that a larger number of particles were retained within the narrower pores. However, the fundamental mechanism of clogging in porous media caused by particle transport was not stated. Liu and Mostaghimi (2017) performed parallel computations on 3D samples using lattice Boltzmann and finite volume methods and simulated dissolution of a carbonate rock sample together with particle migration and reactive transport. Their simulations were conducted under low Peclet regime to study the effect of flow rate on reactive transport. Using image based pore structures, they showed that the resulting permeability-porosity relation from modelling are less accurate when low-resolution images are used for simulations.

Li and Prigiobbe (2018) developed a numerical model by the help of LBM, Immersed Boundary Method (IBM), and Discrete Element Method (DEM). They investigated fine particles motion in porous media using a two-way coupling implemented between fluid flow and fine particles. Their results showed that both particle size and the structure of porous media can influence particle transport and retention. This consequently could alter the flow regime and decrease the permeability. In addition, simulations showed that increase of pressure drop because of the retained particles can promote detachment and allow restoring the initial permeability. Ahkami et al. (2020) studied pore-scale behaviour of mineral precipitation patterns in a fractured porous medium, employing a 2D phase field lattice-Boltzmann method. They introduced a porosity-permeability relation that considered species transport, mineral precipitation and pore space geometry changes. A wide range of diffusivity and reaction rates was explored to study different flow regimes ranging from advection to diffusion-dominated regimes. Their results showed

that permeability reduction is affected by clogging regime close to the flow inlet.They found a linear reduction in permeability for the fracture isolation regime when the precipitation reactions narrowed down the fractures, and permeability reduced slowly in the diffusive precipitation regime where precipitation reactions spread between solid grains. In order to a better understanding of grain detachment and migration during reactive flow, Liu et al. (2020) studied the effect of permeable grain boundaries on dissolution of carbonate rock with complex structure and porosities by a 2D grain-scale modelling. Their results showed a decrease in permeability due to the clogging of transport pathways caused by grain detachment. In addition, they found that an increase in flow rate causes a reduction in detachment and fracture clogging by reducing local dissolution along grain boundaries.

Parvan et al. (2020) investigated the influence of initial porosity and different topology on the porosity-permeability relationship using LBM for fluid flow simulation. Six real geometries were used to evaluate the clogging process. Three geometries with identical topologies but different initial porosities were used for investigating the influences of porous media geometrical effect and an extra three samples, for which the solid grain were repositioned, were used to study the porous media topological effects. In our previous study (Parvan et al., 2020), we explored the dependency of clogging on both porous media geometrical and topological propertiesby only considering particle attachment. In this article, in addition to particle attachment, we include detachment of particlesto explore its impact porous media clogging.Particle detachment isimplemented by computing a critical shear force at the surfaces of solid grains. Several hydrodynamicalparameters are presented at the pore scale and the results are compared between simulations with and without particle detachment process. The findings are explained by providing fluid velocity fields, distribution of shear forces, and particle attachment and how these are affected when particle detachment in included. Finally, to show the influence of particle detachment at the larger sample scale, we explored the effect of detachment process on coefficients of Carman-Kozeny relation and how these coefficients change during adsorptive transport for simulations with and without detachment process.

2. Methodology and modelling assumptions

To simulate fluid flow and particle transport, including attachment and detachment of fine particles, we have considered two sequential steps in our simulations. First, fluid flow is simulated to obtain a steady state flow for a given pore structure. The pore structure is determined by the initial pore geometry as well as the subsequent attachment/detachment of particles changing the pore structure. In a second step, using the established flow, particle transport including attachment and detachment processes are simulated.

The challenges encountered in lattice Boltzmann modelling of complex geometries are two folds. First, the representation of the complex geometry in the Cartesian grid does not conform to the curved boundaries. Secondly, in implementing the boundary conditions, inaccurate distribution functions originated from the solid nodes may be generated during the streaming operation. In our study, the complex geometry is converted into binary data before the numerical solution. The no-slip boundary conditions are included using the Standard Bounce Back (SBB) scheme in this study. SBB scheme reverses the distribution functions at the stationary solid surfaces and is used very often in LBM method to represent the non-slip boundary conditions. It reverses and sends back the distribution functions penetrated to the stationary solid surface. For our simulations, we have combined the LBM (for flow simulation) with a Lagrangian method for particle transport simulation in porous media. The following assumptions have been considered for particles motion during attachment and detachment processes: a) through the simulations, physical properties of fluid such as its dynamic viscosity and densityare unaffected because the concentration of the point particles in the fluid is sufficiently low. b) Particle transport and particle detachment occur due to hydrodynamic drag forces and hydrodynamic shear force, respectively, and mechanism including interactions between fine particles, gravity, van der Waals forces, and electrostatic double layer forces are not considered. This assumption is often made in studies considering horizontal flow (Feng et al., 2015;Bagalkot and Kumar, 2018;parvan et al., 2020) which is consistent with our simulations. c) the injected particles have small size relative to the pore size, and, therefore, their effect on fluid flow regime is negligible up to their deposition time (after which the flow field is solved and velocities are updated accordingly). d) The distance between the surface of particles and grain boundaries are used as a measure for attachment and detachment of fine particles through defining a critical value for hydrodynamic shear force.

3. Mathematical model

3.1. Fluid flow simulations

LBM is an effective approach for numerical simulations of fluid flow, which has been used in diverse studies (Succi, 2001; Sukop and Thorne, 2006; Aidun and Clausen, 2010, Parvan et al., 2019) including pore-scale simulation of flow through different porous media (Koponen et al. 1998; Koivu et al. 2009; Mattila et al. 2016). LBMis a mesoscopic numerical method that can bridge the micro and the macro scales. In LBM, the fluid flow is solved based on discrete version of the Boltzmann equation. Often bounce-back algorithm is used in LBM to apply no-slip boundary condition at the interface of fluid and solid grains. In this study, the D2Q9 scheme is used and at each time step, LBM equations are solved in a transient form until steady-state flow is reached. The LBM for fluid flow is described by the following discretized Boltzmann equation:

$$f_\alpha\left(\mathbf{x}+\mathbf{c}_{\boldsymbol{\alpha}}\Delta t, t+\Delta t\right)-f_\alpha(\mathbf{x},t)=-\frac{f_\alpha(\mathbf{x},t)-f_\alpha^{eq}(\mathbf{x},t)}{\tau} \tag{1}$$

here,f_α is Boltzmann distribution function to calculate density and velocity field and f_α^{eq} is distribution function in equilibrium state used for direction α. In addition, τ and $\boldsymbol{c_\alpha}$ mention hydrodynamic relaxation time and velocity vector in α-direction, respectively.These parameters are expressed as:

$$f_\alpha^{eq}=\omega_\alpha\rho\left[1+3\frac{\mathbf{c}_{\boldsymbol{\alpha}}.\mathbf{u}}{C^2}+\frac{9}{2}\frac{\left(\mathbf{c}_{\boldsymbol{\alpha}}.\mathbf{u}\right)^2}{C^4}-\frac{3}{2}\frac{\mathbf{u}.\mathbf{u}}{C^2}\right] \tag{2}$$

here $C=\Delta x/\Delta t$ is related to the lattice sound speed. Δx and Δt are lattice length and lattice time that both are selected as 1, and ω_α is the weight coefficient for the α-direction expressed as:

$$\omega_\alpha=\begin{cases}\frac{4}{9}\alpha=0\\ \frac{1}{9}\alpha=1,2,3,4\\ \frac{1}{36}\alpha=5,6,7,8\end{cases} \tag{3}$$

$$\tau=\frac{\upsilon}{C_s^2}+0.5 \tag{4}$$

$$\mathbf{c}_{\boldsymbol{\alpha}}=\begin{cases}0\ \alpha=0\\ \left(\cos\left[(\pi(\alpha-1)/2)\right],\sin\left[(\pi(\alpha-1)/2\right]\right)C\alpha=1,2,3,4\\ \left(\cos\left[(\pi(\alpha-4-1)/2)/2\right],\sin\left[(\pi(\alpha-4-1)/2)/2\right]\right)\sqrt{2}\alpha=5,6,7,8\end{cases} \tag{5}$$

where $Cs=C/\sqrt{3}$ and υ are sound speed and kinematic viscosity, respectively. The macroscopic variables of fluid, such as density $\rho(\boldsymbol{x},\ t)$ and velocity $\mathbf{u}(\boldsymbol{x},\ t)$ can be calculated by using of:

$$\rho(\mathbf{x},t)=\sum_\alpha f_\alpha(\mathbf{x},t) \tag{6}$$

$$\mathbf{u}(\mathbf{x},\mathrm{t})=\frac{\sum_\alpha \mathrm{f}_\alpha(\mathbf{x},\mathrm{t})\mathbf{c}_{\boldsymbol{\alpha}}}{\rho(\mathbf{x},\mathrm{t})} \tag{7}$$

3.2. Implemented boundary conditions

In present simulations, a non-slip boundary condition is applied for top and bottom boundaries and a periodic boundary condition is used at the inlet and the outlet boundaries. The unknown distribution functions in D2Q9 lattice arrangement for each boundary are computed as:

$$\text{top boundary (bounce back)}: \begin{cases} f_4(i,ny) = f_2(i,ny) \\ f_7(i,ny) = f_5(i,ny) \\ f_8(i,ny) = f_6(i,ny) \end{cases} \quad (8)$$

$$\text{bottom boundary (bounce back)}: \begin{cases} f_2(i,1) = f_4(i,1) \\ f_5(i,1) = f_7(i,1) \\ f_6(i,1) = f_8(i,1) \end{cases} \quad (9)$$

$$\text{inlet boundary (periodic)}: \begin{cases} f_1(1,j) = f_1(nx,j) \\ f_5(1,j) = f_5(nx,j) \\ f_8(1,j) = f_8(nx,j) \end{cases} \quad (10)$$

$$\text{outlet boundary (periodic)}: \begin{cases} f_3(nx,j) = f_3(1,j) \\ f_6(nx,j) = f_6(1,j) \\ f_7(nx,j) = f_7(1,j) \end{cases} \quad (11)$$

where *i, j,nx*, and *ny* are the horizontal node indices, the vertical node indices, the number of lattice nodes in the horizontal direction, and the number of lattice nodes in the vertical direction, respectively. Moreover, the fluid flow is driven by an extremely small body force on the fluid.

3.3. Simulating particle transport

The motion of a particle in the flow field occurs in the Lagrangian simulation step in response to the hydrodynamics drag forces. The Lagrangian equation of motion of a particle suspended in a fluid is given as:

$$m\frac{d\mathrm{v}}{dt} = F_D \quad (12)$$

where m is the mass of particle, v is particle velocity, and F_D is hydrodynamic drag force. The actual diameter size of the injected fine particles and the average grain diameter are 0.608 μm and 35-40 μm, respectively. When the Reynolds number of the domain is low and the particle is not close to the channel wall, the Stokes drag force effects on the particle can be expressed as (Stokes, 1850; Horwitz and Mani, 2016; Horwitz and Mani, 2018; Qiu, 2015):

$$F_D = 6\pi\mu a_c(u - v) \quad (13)$$

whereμ is dynamic viscosity,a_c is particle radius, u fluid velocity, and v is particle velocity.

3.4. Attachment mechanism

After fluid flow simulation, hydrodynamic drag force is implemented on the existing particles which include the attached particles at the solid boundaries as well as the suspended particle in the fluid phase. The attachment of fine particles at the solid boundaries of grains during their transport could ultimately cause permeability reduction and clogging of the pores. If conditions for clogging are favourable, porous media becomes completely clogged and its permeability approaches zero. In this research, the distance between the surface of colloid and the boundary of grains was used as the main criterion to determine particle settlement. If the distance between the fine colloid and grain boundary is equal or lower than the assumed particle radius, the fine particle is considered as attached to the grain surface. When the accumulated volume of attached particles in a numerical cell exceeds 90% of the cell volume that fluid cell is converted from fluid into a solid phase cell and the pore structure is updated accordingly. The deposited particles can, however, detach in the presence of sufficient shear rate and the pore spaces reopen (Parvan et al., 2020).

Table 1
Proposed formulations to calculate shear force at the solid-fluid interfaces.

$\sigma = 3C\pi\mu D_P\, v$ (14)	Shear stress on deposited particles
$\sigma_f = \sigma_{cr} = C_f F_N$ (15)	Gupta and Civan (1994)
$\sigma_{cr} = k_t c_p^{\alpha}$ (16)	Civan (1990, 1996a)
$\sigma_{cr} = \frac{H}{24D_P l^2}$ (17)	Potanin and Uriev (1991)
$\sigma_{cr} = \rho v_{cr}^2$ (18)	Tremblay et al. (1998)

3.5. Detachment mechanism

In the presence of fluid flow, when the shear force next to the surface of the deposited colloid increases and passes a critical value, particle release and re-entering into the balk fluid takes place. Some of the methods for computing the shear force on the boundary of solid grains are expressed in Table 1:

In Eq. (14), σ is shear stress, and C is used to account for deviation from a sphere shape, and μ, D_P and v are the fluid viscosity, particle diameter and interstitial fluid velocity, respectively. The direction of the interstitial fluid flow is parallel to solid the surface.

A friction force is considered in Eq. (15) to compute the critical shear forces between the attached particles and the pore surface. This value could be additionally considered as a criterion for particle detachment. F_N is adhesive force acting on the deposited particles which results from summation of hydrodynamic force and including viscous drag force and DLVO forces. The latter includes attractive Lifshitz-van der Waals and electrostatic double layer forces acting on the deposited particles. The parameter C_f denotes a friction coefficient which is different for rolling, sliding or other forms of particle motion. In Eq. (16), Civan (1990, 1996a) considered a critical shear stress, where k_t denotes the particle stickiness to surface, and c_p and α are particle mass concentration and an empirical constant, respectively. The critical shear stress predicted by Potanin and Uriev (1991) is based on the interactive van der Waals energy between solid phases in the filter cake (Eq. (17)). In this relation, H is the Hamaker coefficient, D_P and l are the average particle diameter and the separation distance between the particle surfaces in filter cake, respectively. Tremblay et al. (1998) developed a critical condition for onset of particle mobilization by fluid shear based on the study of Yalin and Karahan (1979), and provided the following relation:

$$N_{M_{cr}} = 0.122 N_{Re_{cr}}^{a} \quad (19)$$

where a is -0.206 and $N_{M_{cr}}$ and $N_{Re_{cr}}$ are the critical mobility number and the critical Reynolds number, respectively. These parameters can be expressed as:

$$N_{M_{cr}} = \frac{\rho v_{cr}^2}{\gamma_s D_P} \quad (20)$$

$$N_{Re_{cr}} = \frac{\rho v_{cr} D_P}{\mu} \quad (21)$$

where v_{cr} and γ_s are the critical shear velocity and specific weight of particles suspended in the fluid, respectively. By using Eq. (16) and using dimensionless groups, Tremblay et al. (1998) correlated their experimental data on a full logarithmic scale and introduced a critical shear velocity as:

$$v_{cr} = 0.385\left(\frac{\mu}{\rho}\right)^{a} \gamma_s^{b}\, D_P^{c}\, \rho^{d} \quad (22)$$

where *a, b, c*, and *d* considered 0.0934, 0.453, 0.36, and -0.453,respectively. Then, they predicted the critical shear stress on the surface as:

$$\sigma_{cr} = \rho v_{cr}^2 \quad (23)$$

We used relations developed by Tremblay et al. (1998) mainly because of its simplicity. Using this relation, we obtain the critical shear force needed for particle detachment in the presence of fluid flow.

4. Results and discussions

Simulations are conducted on real geometries from a sand pack with an original porosity of 36%. The geometry of domains was obtained using x-ray tomography method with a resolution of 10 μm. A 2D slice of this image was used as the pore scale domain. Furthermore, a numerical erosion was performed on this 2D slice to generate two extra pore scale domains (i.e., a total of three pore structures) which had similar arrangement of pores and grains but different porosity values. In doing so, to obtain a domain with a desired porosity value the ImageJ package (Rueden et al., 2017) was used and image pixels corresponding to the surface of the solid grains were removed in a layer-by-layer manner for all grains until a desired porosity was obtained for each domain. The physical size of the real porous domain is 380 × 800 μmin horizontal and vertical directions, respectively. The three geometries had initial porosity values of 38.2%, 45.9%, and 52.1%, which we refer to them as samples S1, S2, and S3.

A non-slip boundary condition was applied using a bounce back method at the top and bottom boundaries and the periodic boundary condition was implemented for both the inlet (located at the left side of the domain) and the outlet (positioned at the right side of the domain) boundaries. To prevent the effect of inlet and outlet boundary conditions on fluid flow thorough porous domain, two fluid jackets were considered before and after the inlet and outlet, respectively. Grid independency tests have provided an optimum grid size of 237 × 500 in lattice unit for our porous domain. The relaxation time was assumed to be 0.65 in lattice unit. The parameter values are chosen in the range of natural groundwater and clay particles in the earth subsurface. The bulk density of water is set to 1000 $\frac{kg}{m^3}$ and the density of clay, or clay loam, immersed in groundwater should be between1000 and 1600 $\frac{kg}{m^3}$ (Brady, 1974). In our simulations, colloid transport is driven by the hydrodynamic drag force and since density of colloids (1055 $\frac{kg}{m^3}$) is very close to that of fluid solution, the gravity and buoyancy forces are neglected in this study.

We validated our numerical model against a well-known benchmark problem which uses cylindrical-shape grains and uses Kozeny–Carman equation to calculate permeability as a function of domains porosity (Hommel et al. 2018; Voronov et al, 2010; (Lee and Yang, 1997)):

$$K = \frac{\phi_s^2 D_p^2}{180} \frac{\varphi^3}{(1-\varphi)^2} \tag{24}$$

where φ_s is the sphericity, a dimensionless particle geometry parameter computed from Li et al. (2012), D_p is the characteristic particle diameter, and φ is the porosity.

The results of modeming tests and Carman-Kozeny relation results are provided in Fig. 1.

The validated model was used to perform simulations for particle transport thorough porous domains. The diameter of the injected particles was 0.61 μm and the average grain diameters in three geometries were 40.5, 37.9, and 35.9 micrometres, respectively. Fine particles were injected into the fluid phase at equal distances at the inlet. Since the aim of this study was to explore detachment of the settled particles under different flow regime, we began with applying low velocities in the inlet by using an extremely small body force on fluid, for which no detachment happens. In the subsequent simulations as inlet velocity was increased the critical velocity was found (below which the detachment would not occur). The Reynolds number, $Re = \frac{\rho u D}{\mu}$, based on the inlet fluid velocity and the average grain diameter for these three cases are 0.0005, 0.0009, and 0.0019, respectively. The magnitude of critical velocity was found to be larger for samples with grater initial porosities. This trend could be attributed to the existence of wider pore throats in samples S2 and S3 and lower average velocity values under identical inlet fluid velocity through the pores of these samples. Fig. 2 shows flow velocity distributions for the three pore structures using the same inlet flow velocity. Fig. 3 shows the permeability reduction due to particle attachment during clogging process. Because of the larger initial porosity and fluid flow thorough

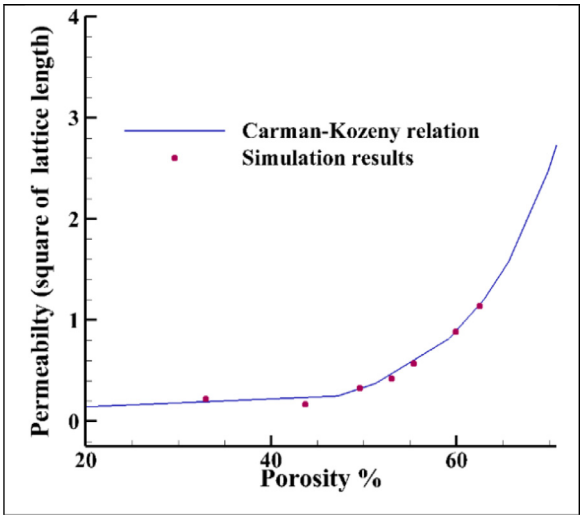

Fig. 1. Predicted permeability values using modelling together with values obtained from Carman-Kozeny relation.

domain S3, attachment occurs almost at the boundary of all grains. In the other two samples (particularlyS1) fluid was transported thorough distinct pathways and the injected fine particles accumulated only in specific zones.

To highlight the influence of particle detachment in domains, for each domain two series of simulations with velocities greater than critical inlet velocities were performed, one by considering detachment process and one without detachment. Fig. 4 shows simulation results for two situations (i.e., with and without detachment). Green regions show zones where particle deposition at grains surfaces is occurred. In this Figure the inlet velocities for sample S1, S2, and S3 are set to 2.8, 4.5, and 8.4 m/day, respectively. The Reynolds number, $Re = \frac{\rho u D}{\mu}$, based on the mean fluid velocity at inlet and the average grain diameter for all three cases are 0.0013, 0.0019, and 0.0034, respectively. Particle detachment caused obvious differences between pore structures and simulation results while considering or neglecting the detachment. For better visualization and comparison, yellow frames are sketched in the sample with initial porosity of 38.2%. In sample S1, due to the low initial porosity, clogging could occur fast, but detachment delays clogging and because of this reason, the attached particles in the final geometry in the state with detachment are more than the state without detachment. In sample with initial porosity of 45.9% it is obvious that in the state without detachment, attachment occurs in the whole domain but due to detachment process in other state, attachment has almost negligible effect.

For sample S1, when detachment was included, clogging occurred in longer period of time, compared to simulations without detachment, and solid particles had more time to deposit at the surface of grains (see Figure S3 for sample S1). In addition, in presence of detachment in sample S1, most of particle deposition took place during time periods close the complete clogging. In cases with detachment in samples S2 and S3, porous geometry was ultimately clogged. However, in cases without detachment, a complete clogging did not occur which allowed the flow to continue and more particles could flow in and attach to the grains surfaces.

In Fig. 5, dimensionless permeability-porosity relation, porosity-time relation, and dimensionless permeability-time relation are provided for different simulations. Variations in physical parameters such as porosity and permeability in sample S1 follow the same trend both with and without detachment included. It is obvious that detachment process delays the clogging (almost by two times) during which lower porosities and permeabilities could be reached. In sample S2, while a complete clogging occurred under no detachment scenario, no significant varia-

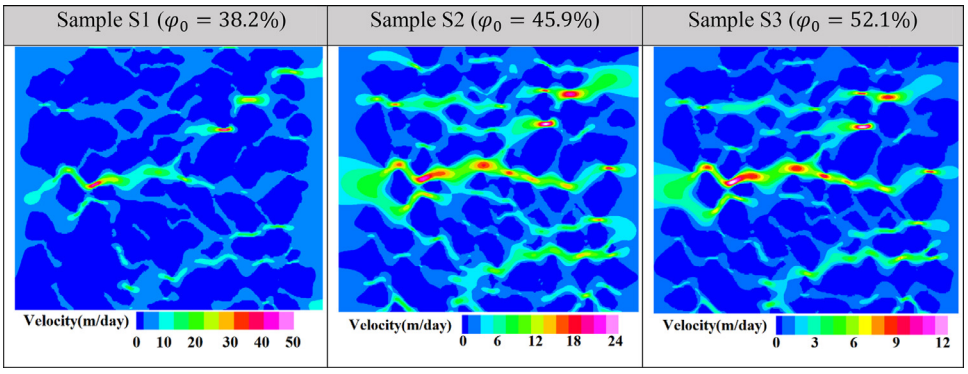

Fig. 2. The flow velocity distribution using an identical inlet fluid velocity applied to domains with different initial porosities. The average fluid velocity in pores of sample S1 is larger than sample S2 and S3 (note different velocity legends for each plot). To observed considerable particle detachment in these three geometries, the inlet flow velocity should be increased for Sample S2 and S3.

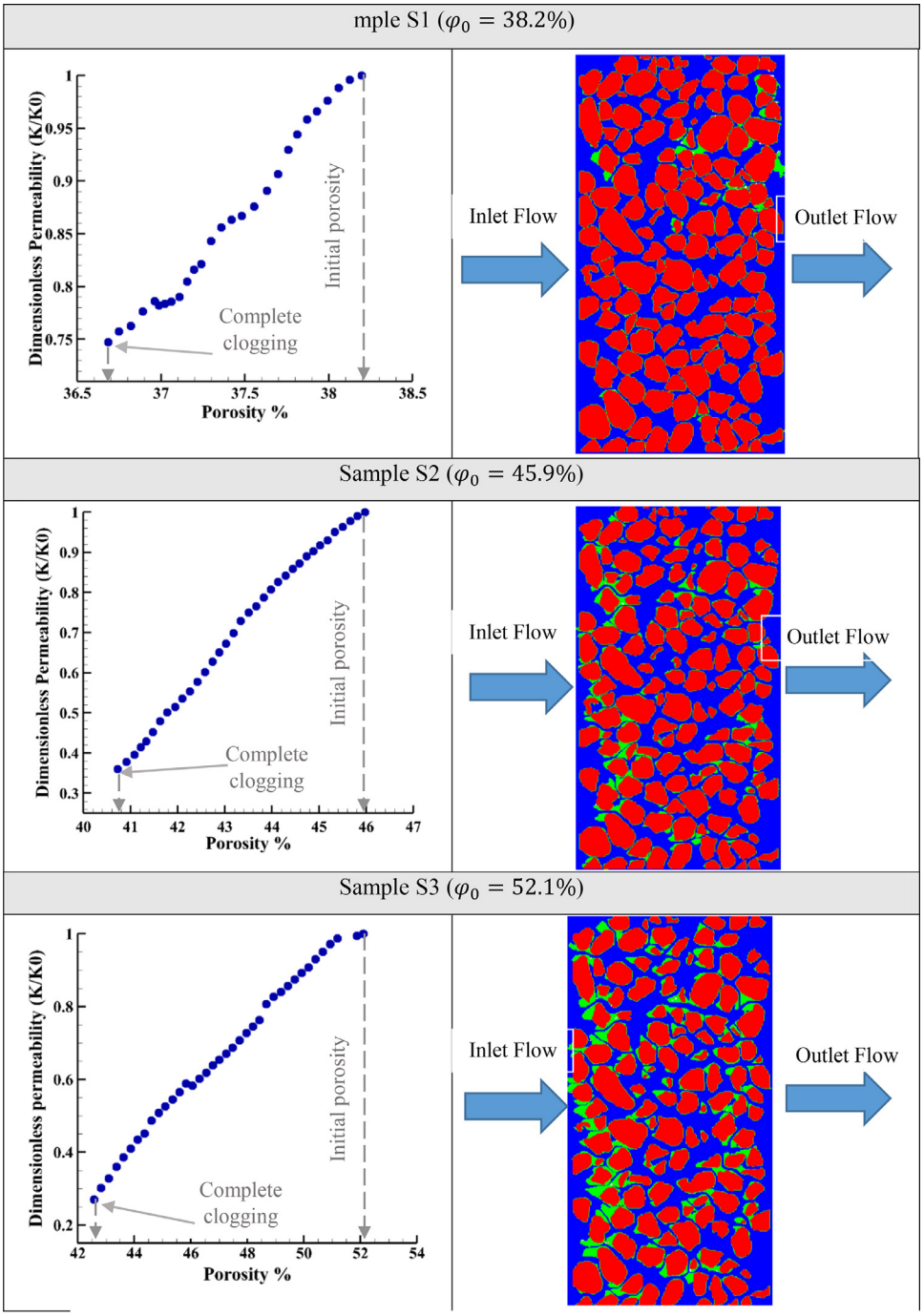

Fig. 3. Porosity-permeability relation for the three geometries (i.e., S1, S2, and S3 with different initial porosities) with and without considering the colloid attachment process. The inlet fluid velocities are 1.2, 2.2 and 4.7 m/day and the initial porosity values are 38.2%, 45.9%, and 52.1%, respectively.

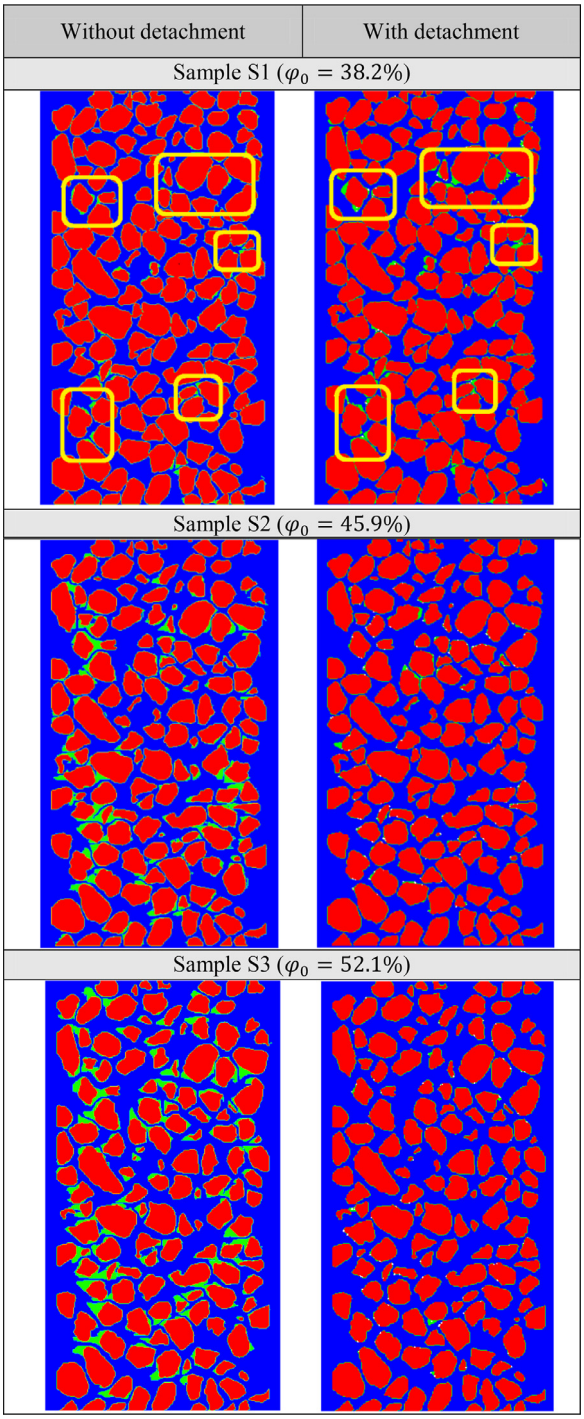

Fig. 4. Pore structures with different geometrical properties in two states. The physical domain sizes were 380μm × 800μm in horizontal and vertical directions, respectively.

tion in porosity and permeability was observed when detachment was included. In sample S3, no variation in porosity and permeability was observed when inducing detachment processes. However, without detachment, both porosity and permeability reduced and complete clogging occurred.

4.1. Fitting simulation data on Carman-Kozeny relation

There are several relations to explain the permeability reduction resulted from a decrease in porosity (Kozeny, 1927; Carman, 1937; Hommel et al., 2018) during particle deposition on grains. One of the well-known relations in this field is Carman-Kozeny relation which we used to fit on our results. We used Carman-Kozeny relation in the form of:

$$\frac{K}{K_0} = a\frac{\left(\frac{\varphi}{\varphi_0}\right)^b}{\left(\frac{1-\varphi}{1-\varphi_0}\right)^c} \tag{25}$$

Where K and K_0 are permeability and initial permeability and ϕ and ϕ_0 are porosity and initial porosity, respectively. Parameters ***a, b***, and ***c*** in this relation have been fitted to present relation between porosity and permeability based on Carman-Kozeny relation. This procedure was repeated for different simulations to investigate the impact of detachment process on these coefficients. Values are provided in Table 2:

Table 2
The fitted coefficients of Carman-Kozeny relation to the pore scale simulation data with and without considering the detachment process.

	With detachment	Without detachment
Sample S1(ϕ_0 = 38.2 %)		
a	1.013	1.005
b	29.69	49.12
c	-37.62	-67.32
Sample S2(ϕ_0 = 45.9 %)		
a	0.998	0.999
b	145.40	32.54
c	-174.1	-33.92
Sample S3(ϕ_0 = 52.1 %)		
a	0.999	1.006
b	216.00	12.33
c	-199.80	-7.85

The value of these parameters depends on different factors such as fluid flow properties, specific surface area, tortuosity, sphericity, particle diameter, etc. The value of coefficient ***a*** in all samples for with detachment and without detachment are almost 1, but there are differences in other parameters. The magnitudes of ***b*** and ***c*** parameters decrease with an increase in initial porosity for without detachment state, but these values are increased for the with detachment state. It is notable that the difference between the magnitudes of both parameters ***b*** and ***c*** is increased with an increase in initial porosity. It can be related to the increase in detachment influence in samples with higher initial porosities.

4.2. Detachment effect on velocity distribution

Fig. 6 shows the fluid velocity distribution and facilitates the evaluation of the detachment effect on fluid velocity and the maximum fluid flow in the last step of simulation process. The inlet fluid flow velocity for samples S1, S2, and S3 are 2.8, 4.5, and 8.4 m/day, respectively. According to this figure, although sample S1 has the lower inlet velocity, the fluid flow velocity in its pore throats is higher than others. Because of high detachment intensity in sample S2 and S3, fluid velocity in their pore throats cannot exceed too much. Detachment intensity in sample S2 and S3 is not very different and due to the higher inlet velocity, the maximum fluid velocity value in sample S3 is more than its value in sample S2. The unaffected pore structures of samples S2 and S3 helps these samples to maintain their flow pathways over time. Fig. 6 shows that major flow pathways are approximatelythe same in all samples and parameters such as inlet flow velocity, difference in initial porosities, and particle attachment/detachment did not affect them significantly.

Fig. 7 shows the average fluid velocity histogram of three samples. The behaviour of sample S1 varies over time, while samples S2 and S3 does not show any significant changes in their porous structures and their average fluid velocities (calculated at successive cross sections) is

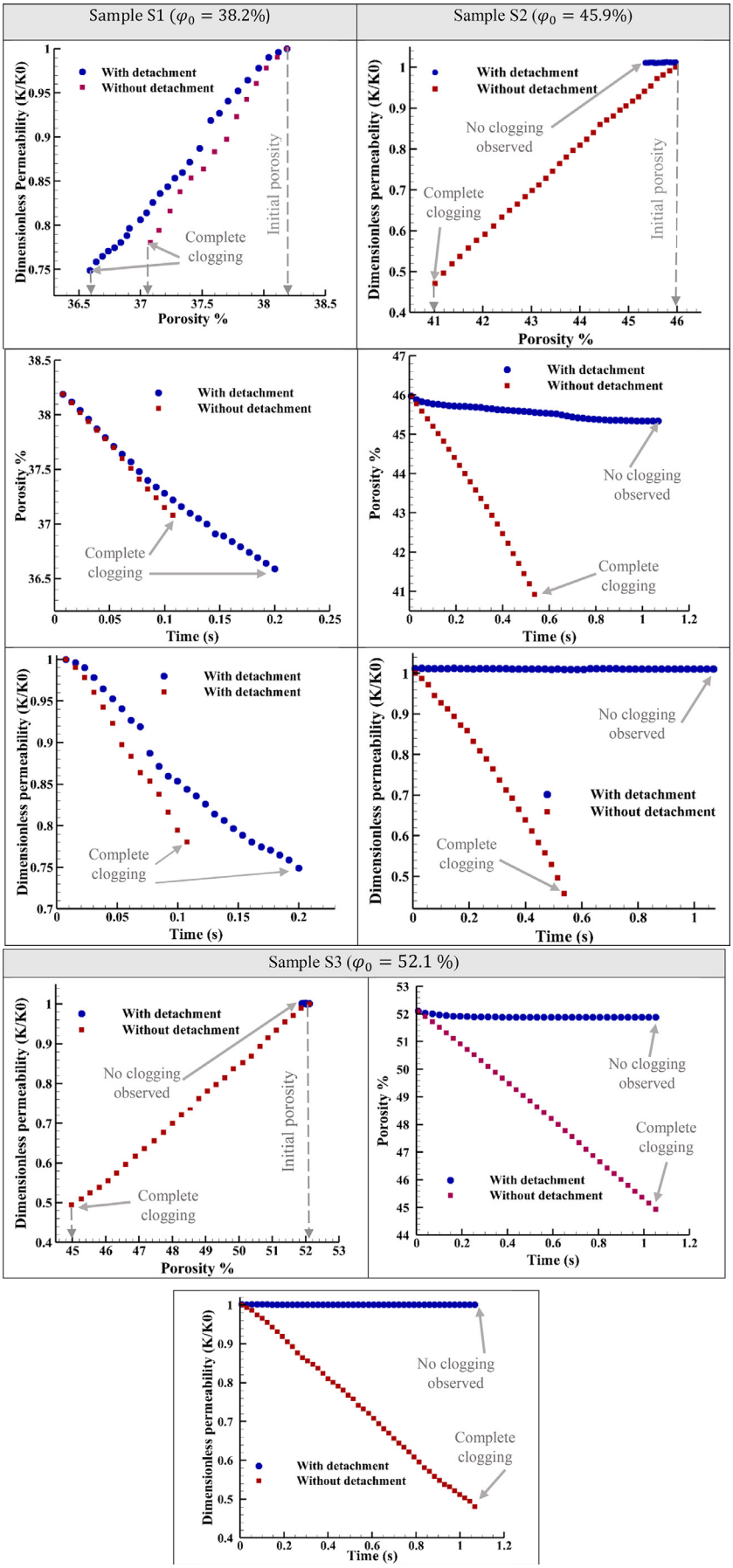

Fig. 5. Porosity-permeability, porosity-time, and permeability-time relations for sample S3 geometries with different initial porosity.

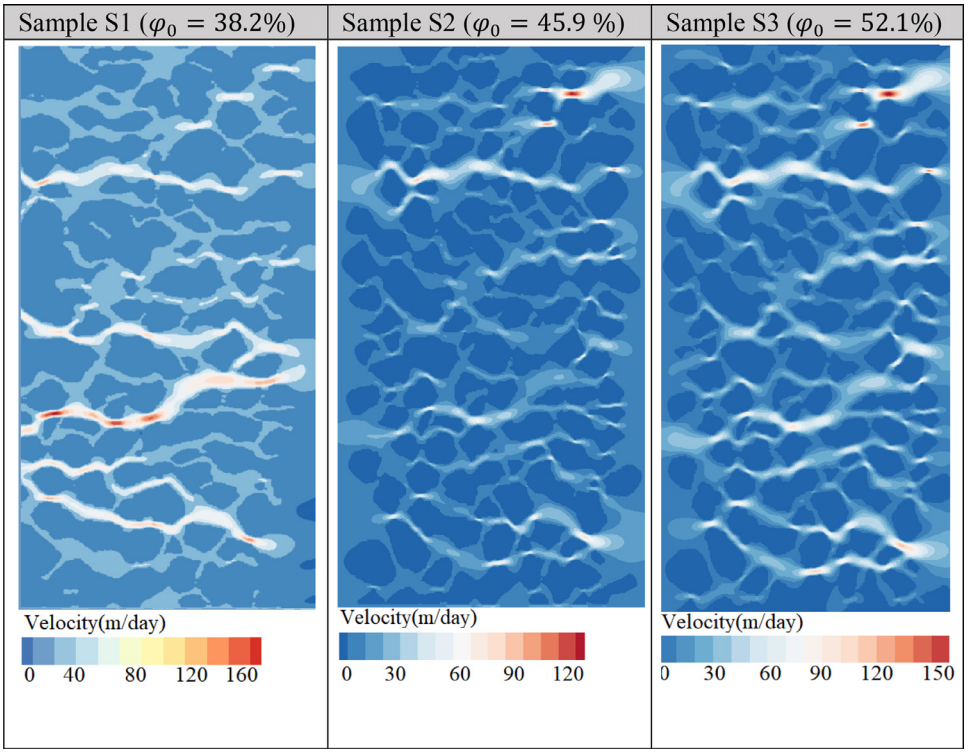

Fig. 6. Fluid velocity distributions for three geometries with different initial porosities in the presence of detachment process.

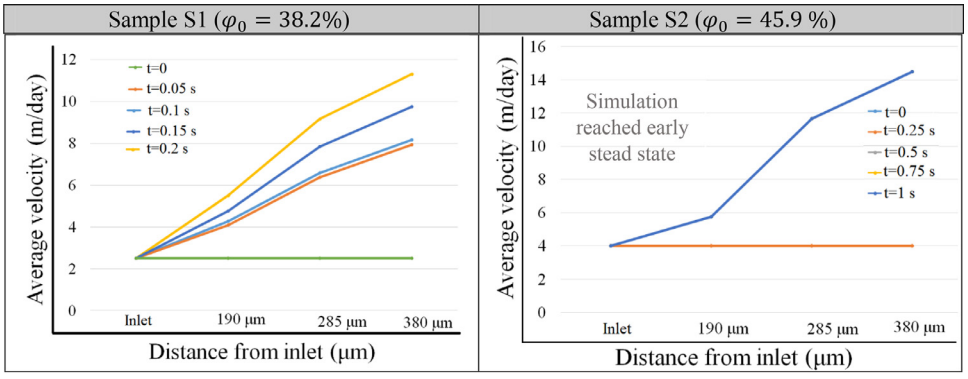

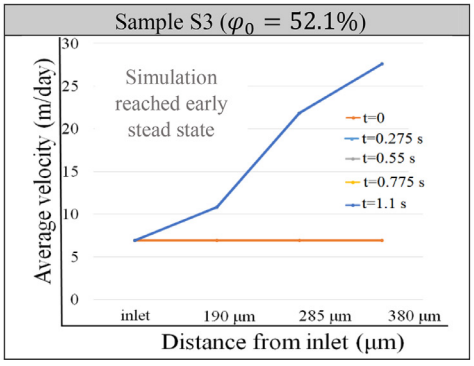

Fig. 7. Cross-sectional averaged velocities obtained at several longitudinal distances from the inlet (i.e., at 0.0, 190, 285, and 380 μm) for all three samples. Sample S1 shows a transient behaviour in the detachment process resulting in different profiles of velocity over time. Samples S2 and S3 reached to steady-state conditions where the velocity filed stayed unchanged over time. Due to relatively uniform grain distributions (i.e., macroscopically homogeneous samples) all sample show an initially uniform cross-sectionally averaged velocity values across the samples.

unchanged over time. In all three samples, because of the porous geometry of the domain, the average fluid velocities near the outlet are greater than the inlet. Geometry changes of sample S1 (due to particle attachment and particle detachment) causes variations in sample cross sections with time, and, therefore, the average fluid velocity grows in this sample.

4.3. Detachment effects and adsorbed mass along porous domains

During flow, a fraction of the injected particles reach to the outlet boundary and exit porous domain, while the rest of particles deposit on the solid grain surfaces. A fraction of the deposited fine particles are detached and may redeposit on other solid grain located downstream of the flow and some of them may exit the domain. The detachment process

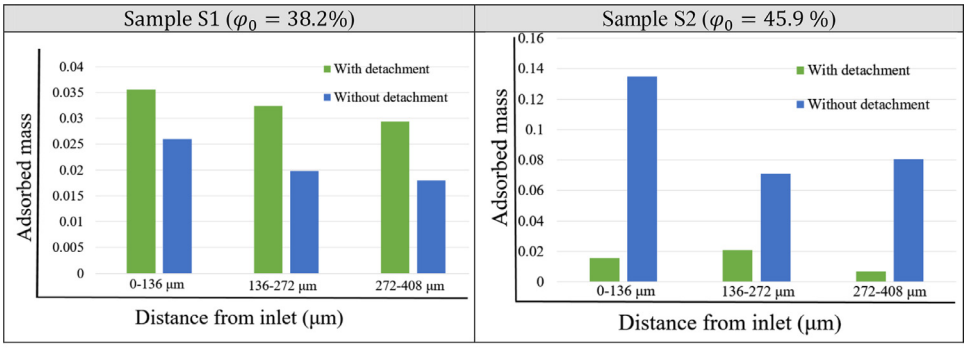

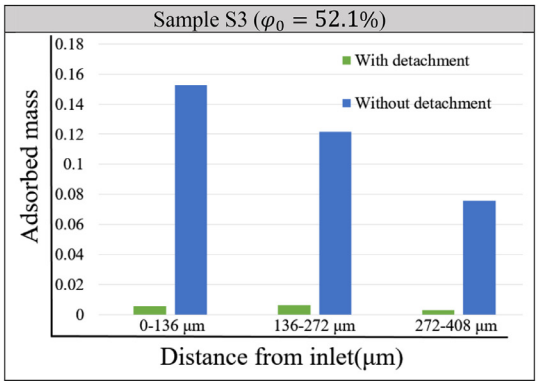

Fig. 8. Amount of absorbed mass at different longitudinal regions from the inlet (i.e., at regions with sizes 0-136, 136-272, and 272-408 µm). The regions are chosen to represent the initial, middle, and end regions of the porous media samples.

can postpone or prevent porous media clogging, and, in some cases, fluid flow paths are considerably affected by the detached and attached particles. Fig. 7 shows the adsorbed mass (i.e., due to particle attachment) in different locations of porous domains along the flow when sorption is with and without detachment process at the solid grains. Remarkably, in the sample with initial porosity of 38.2% (i.e., S1) the adsorbed mass, when particle detachment is included, is larger compared to the attached mass without detachment. This behaviour is because, the detachment process postpones complete clogging of the media (by remobilizing a fraction of the attached particles) which enables the fluid flow to continue for longer times and more particles will enter into the domain and attach on solid grains. Without possibility for detachment, the pore structure is clogged at the earlier stages and flow is terminated. Fig. 8 also shows that for the sample with initial porosity of 38.2% (i.e. sample S1), more fine particles deposited near the inlet. In samples with initial porosity of 45.9% and 52.1%, because of higher initial porosity and higher inlet velocity, detachment prevents strong clogging and attachment of fine particle occurs rather uniformly throughout the domain. However, without detachment, the density of attached mass is larger at regions closer to the inlet of the porous media.

4.4. Evaluation of shear force in porous domain

For better visualization of detachment in the samples, Fig. 9 is sketched to show the distribution of shear forces in porous domains. Due to the lower initial porosity and inlet fluid velocity, the value of shear forces in sample S1 are lower than sample S2 and S3. Although the inlet fluid velocity in sample S3 is almost two times greater than sample S2, there is no significant difference in the values of shear force between them. It can be concluded that the initial structure of porous domain has more effective influence on detachment phenomenon than inlet fluid velocity. It is obvious that in addition to lower maximum shear force in sample, the average shear force in many pores is low and detachment cannot occur. By comparing Figs. 9 and 6, we can conclude that in all samples, there is a main path flow and detached particles are related to this path flow.

As change of porosity modifies the flow field, the flow-induced stress tensor $\underline{\tau}$ can be utilized to evaluate this modification (Pham et al, 2014):

$$\underline{\tau} = \frac{1}{2}\mu\left(\nabla u + \nabla u^T\right) \tag{26}$$

where$\mu$is the dynamic viscosity of the fluid and u is the velocity vector. The calculation of the probability distribution function of the fluid stresses in the pore space excluded the surface stresses on the fluid-solid interfaces. Eq. (26) is normalized by subtracting the mean stress, τ, and dividing by the standard deviation, σ_t, of the stress distribution as follows (Porter et al., 2005):

$$\tau^* = \frac{\underline{\tau} - \bar{\tau}}{\sigma_t} \tag{27}$$

Fig. 10 provides the probability distribution function of the normalized shear stress in three porous domains. The difference in the number of modes might be attributed to the non-uniformity of the pore sizes.

Using distributions shown in Fig. 10, it is possible to estimate probability of finding a certain range of stress in the flow field for a given porous.

In Fig. 11, the average shear forces at some cross sections are sketched. The values of average shear forces do not vary during all simulations. The rate of the variations of average shear forces is identical in three samples. The highest shear forces occur near the outlet. We can conclude that, compared to inlet fluid velocity, the average shear forces depend more on initial pore structure.

4.5. Detachment intensity in porous domains

In Fig. 12, the frequency of detached cells has been sketched. It is notable that detachment may occur in each detached cell more than one time. In all cases, the higher intensity of detachment occurs in the second half of porous domains (the third and fourth quarters). In sample with initial porosity of 38.2%, the minimum detachment occurs near to the inlet, but in other two samples the minimum detachment occurs in the second quarter of porous domain. By considering Figs. 9 and 12, it

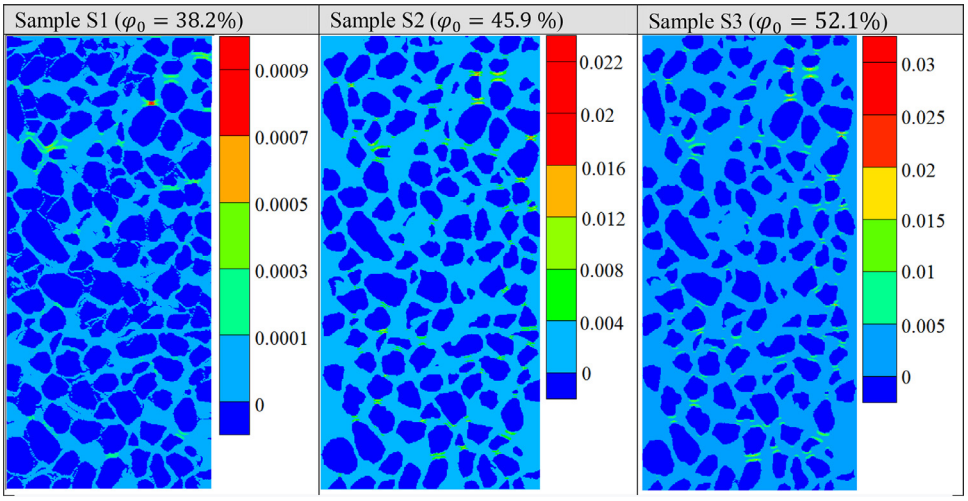

Fig. 9. Simulation results showing the spatial distribution of shear forces in all three porous media domains. Plots S1, S2, and S3 show that shear forces (responsible for particles detachment) are much localized and are present at the location of certain pore throats which have large velocities due to their size as well as their spatial locations within the pore network.

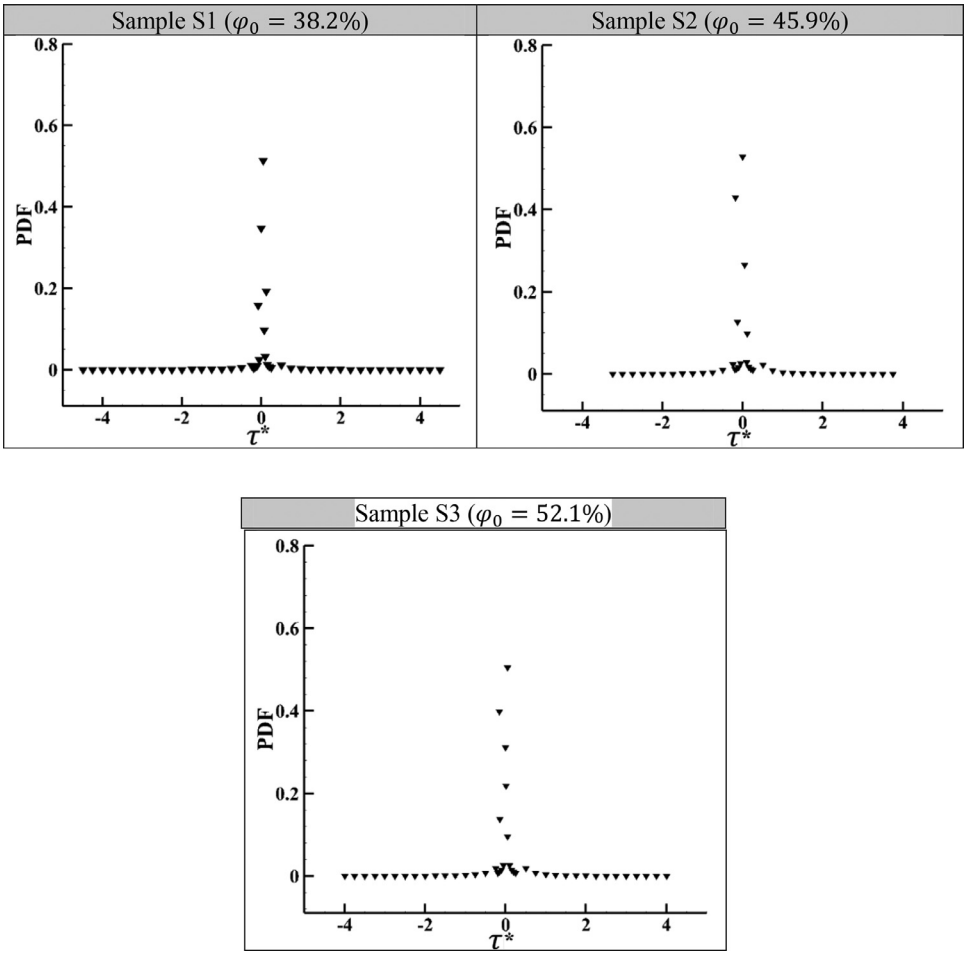

Fig. 10. Normalized stress distributions of three tested porous domains.

can be concluded that the detachment pattern follow the geometry and initial porous domain of porous domain more than fluid inlet velocity.

In addition, the most detachment in all samples occurs exactly in the same zones that we have the most shear stress in the final third of domains. By comparing Figs. 8 and 11, it is found that in zones with lower detachment, more particles are attached to the boundary of solid grains.

5. Summery and conclusion

Porosity and permeability of porous media are changed due to attachment and detachment of moving particles at the fluid-solid interfaces. In this study, the importance of particle detachment and its effects on fluid flow and change of solid structures was explored. Three real porous media samples with identical topological properties, but with

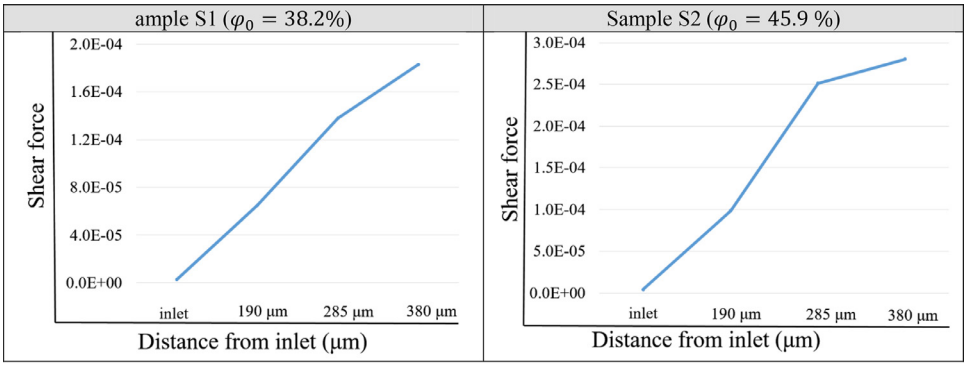

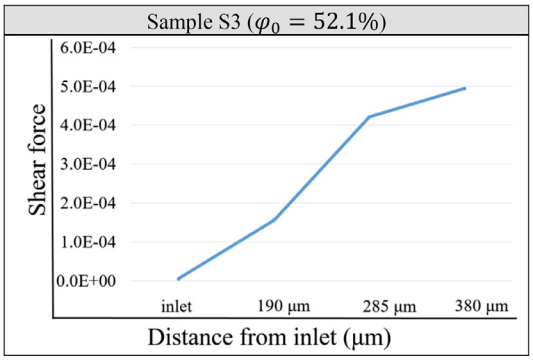

Fig. 11. Cross-sectional averaged shear force obtained at several longitudinal distances from the inlet (i.e., at 0, 190, 285, and 380 µm) for all three samples. All samples reached to steady-state condition where the shear force stayed unchanged over time.

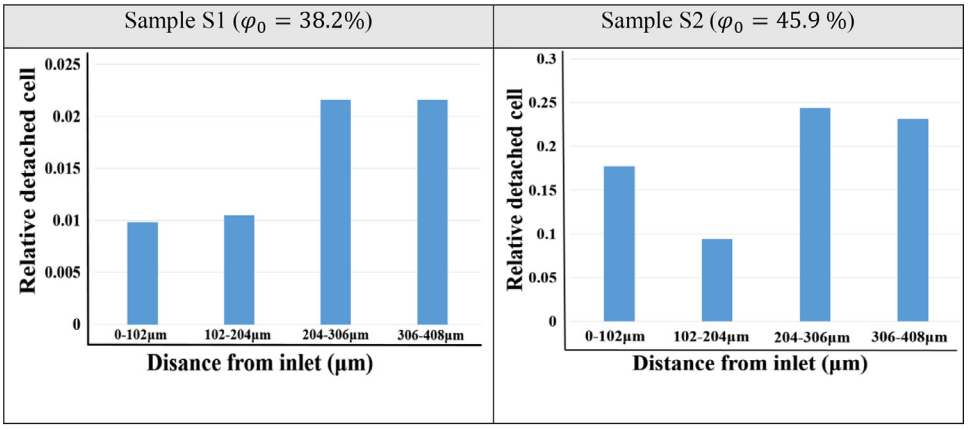

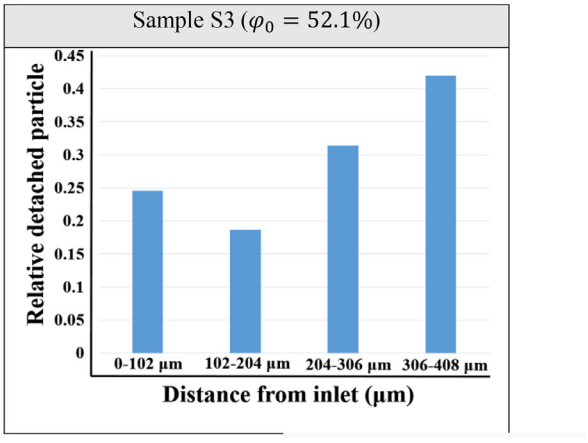

Fig. 12. The detached particles in the four parts of porous domain.

different initial porosities of 38.2, 45.9, and 52.1% were considered. Our main results have shown that:

- A wide range of pore velocities with large values (relative to the average pore velocities) exist within a subset of pore throats. The distributed large velocities resulted in creation of highly localized shear forces with magnitudes larger than the critical value needed for colloid detachment.
- The initial porosity significantly impacts the location and distribution of large velocity location and shear forces and influenced the detachment behaviour. The sample with lower initial porosity value showed a transient behaviour developing to the complete clogging of the sample. Samples with larger initial porosity values reached to early state-state behaviour with no clogging of the media. Samples with larger initial porosities required higher average velocities to generate sufficiently large shear forces for particle detachment.
- Neglecting particle detachment results in early clogging events (since detachment is absent to re-mobilize some of the attached particles and to re-open the pore space) and also impacts the form of porosity-permeability relation. Our resultsshow that coefficients of the porosity-permeability relation are more sensitive to particle detachment for samples with larger initial porosities. In General, particle detachment significantly influenced coefficients $\boldsymbol{b}$ and $\boldsymbol{c}$ of the Carman-Kozeny relation and coefficient $\boldsymbol{a}$ showed negligible sensitivity.
- Including particle detachment affects the pattern and distribution of the attached mass. Porous media with larger initial porosities showed relatively lower detachment and the detached mass was concentrated within the downstream locations of the sample.

Author Statement

Amin parvan: Conceptualization, Methodology, Software, Writing-Original draft preparation, Writing-Reviewing and Editing. **SaeedJafari**: Conceptualization, Methodology, Software, Writing-Reviewing and Editing, Supervision. **MohamadRahnama**: Conceptualization, Supervision. **SaeidNorouziApourvary:** Conceptualization, Methodology, Writing-Reviewing and Editing. **Amir Raoof**: Conceptualization, Methodology, Writing-Reviewing and Editing.

All authors confirm that this paper has not been submitted to any other journals. It should be mentioned that all of authors agree to submit this manuscript to Advances in Water Resources. They also confirmed that this manuscript is their original work.

Declaration of Competing Interest

The authors declare that they have no known competing financial interests or personal relationships that could have appeared to influence the work reported in this paper.

Supplementary materials

Supplementary material associated with this article can be found, in the online version, at doi:10.1016/j.advwatres.2021.103888.

References

Abdul Mujeebu, M., Abdullah, M.Z., Abu Bakar, M.Z., Mohamad, A.A., Abdullah, M.K, 2009. Applications of porous media combustion technology-a review. Appl. Energy 86 (9), 1365–1375. https://doi.org/10.1016/j.apenergy.2009.01.017.

Ahfir, N.D., Hammadi, A., Alem, A., Wang, H.Q., Le Bras, G., Ouahbi, T., 2016. Porous media grain size distribution and hydrodynamic forces effects on transport and deposition of suspended particles. Int. J. Environ. Sci. Tech. https://doi.org/10.1016/j.jes.2016.01.032.

Ahkami, M., Parmigiani, A., Di Palma, P., Roberto, S, Martin, O.K., Xiang, Z., 2020. A lattice-Boltzmann study of permeability-porosity relationships and mineral precipitation patterns in fractured porous media. Comp. Geosci. https://doi.org/10.1007/s10596-019-09926-4.

Aidun, C.K., Clausen, J.R., 2010. Lattice-Boltzmann method for complex flows. Ann. Rev. Fluid Mech. 42, 439–472.

Bacci, G., Korre, A., Durucan, S., 2011. Experimental investigation into salt precipitation during CO2 injection in saline aquifers. Energy Procedia 4, 44504456. https://doi.org/10.1016/j.egypro.2011.02.399.

Bagalkot, N., Kumar, G., 2018. Colloid Transport in a Single Fracture–Matrix System: Gravity Effects, Influence of Colloid Size and Density. Water 10 (11), 1531. https://doi.org/10.3390/w10111531.

Bedrikovetsky, P., Siqueira, F.D., Furtado, C.A., Souza, A.L.S, 2011. Modified particle detachment model for colloidal transport in porous media. Transport in Porous Media 86 (2), 353–383. https://doi.org/10.1007/s11242-010-9626-4.

Bedrikovetsky, P., Zeinijahromi, A., Siqueira, F.D., Furtado, C.A., de Souza, A.L.S., 2012. Particle Detachment Under Velocity Alternation During Suspension Transport in Porous Media. Transport in Porous Media 91, 173–197. https://doi.org/10.1007/s11242-011-9839-1.

Benioug, M., Golfier, F., Oltean, C., Bues, M.A., Bahar, T., Cuny, T., 2017. An immersed boundary-lattice Boltzmann model for biofilm growth in porous media. Adv. Water Resour. 107, 65–82. https://doi.org/10.1016/j.advwatres.2017.06.009.

Bergendahl, J., Grasso, D., 2000. Prediction of colloid detachment in a model porous media: hydrodynamics. Chem. Eng. Sci. 55 (9), 1523–1532. https://doi.org/10.1016/S0009-2509(99)00422-4.

Brady, N.C., 1974. Nature and Property of Soils, 8th edn. Publisher: MacMillan Publishing Co., Inc. B0006D800S.

Carman, P.C., 1937. Fluid flow through granular beds. Trans. Am. Inst. Chem. Eng. 15, 150166.

Chequer, L., Al-Shuaili, K., Genolet, L., Behr, A., Kowollik, P., Zeinijahromi, A., 2019. Optimal slug size for enhanced recovery by low-salinity waterflooding due to fines migration. J. Petrol. Sci. Eng. 177, 766–785. https://doi.org/10.1016/j.petrol.2019.02.079.

Chu, X., Li, T., Li, Z., Yan, A., Shen, C. (2019). Transport of Microplastic Particles in Saturated Porous Media. *Water*. 11, 12, 2474. doi:10.3390/w11122474.

Civan, F., 2001. Scale effect on porosity and permeability: kinetics, model, and correlation. AIChE J. 47 (2), 271–287. https://doi.org/10.1002/aic.690470206.

Coronado, M., Diaz-Viera, M.A., 2016. Modeling Fines Migration and Permeability Loss Caused by Low Salinity in Porous Media. J. Petrol. Sci. Eng. https://doi.org/10.1016/j.petrol.2016.12.021.

Cui, X., Liu, Q., Zhang, C., 2017. Detachment Characteristics of Deposited Particles in Porous Medium: Experimentation and Modeling. Transport in Porous Media 119, 633–647. https://doi.org/10.1007/s11242-017-0902-4.

Deo, O., Sumanasooriya, M., Neithalath, N., 2010. Permeability reduction in pervious concretes due to clogging: experiments and modeling. J. Mater. Civil Eng. 22 (7), 741–751. https://doi.org/10.1061/(ASCE)MT.1943-5533.0000079.

Endo Kokubun, M.A., Muntean, A., Radu, F.A., Kumar, K., Pop, I.S., Keilegavlen, E., Spildo, K., 2019. A pore-scale study of transport of inertial particles by water in porous media. Chem. Eng. Sci. 207, 397–409. https://doi.org/10.1016/j.ces.2019.06.036.

Feng, Q., Li, S., Han, X., Wang, S., 2015. Network simulation for formation impairment due to suspended particles in injected water. J. Petrol. Sci. Eng. 133, 384–391. https://doi.org/10.1016/j.petrol.2015.06.027.

Gaebler, H.J., Eberl, H.J., 2018. A simple model of biofilm growth in a porous medium that accounts for detachment and attachment of suspended biomass and their contribution to substrate degradation. Eur. J. Appl. Math. 29 (6), 1110–1140. https://doi.org/10.1017/S0956792518000189.

Han, G., Kwon, T.-H., Lee, J.Y., Jung, J., 2019. Fines migration and pore clogging induced by single- and two-phase fluid flows in porous media: From the perspectives of particle detachment and particle-level forces. Geomech. Energy Environ., 100131 https://doi.org/10.1016/j.gete.2019.100131.

Haque, M.E., Shen, C., Li, T., Chu, H., Wang, H., Li, Z., Huang, Y., 2017. Influence of Biochar on Deposition and Release of Clay Colloids in Saturated Porous Media. J. Environ. Qual. 46, 1480–1488. https://doi.org/10.2134/jeq2017.06.0223.

Hommel, J., Coltman, E., Class, H., 2018. Porosity–Permeability Relations for Evolving Pore Space: A Review with a Focus on (Bio) geochemically Altered Porous Media. Transport in Porous Media 124, 589–629. https://doi.org/10.1007/s11242-018-1086-2.

Horwitz, J.A.K., Mani, A, 2016. 2016) accurate calculation of stokes drag for point-particle tracking in two-way coupled flows. J. Comput. Phys.318 85–109.

Horwitz, J.A.K., Mani, A, 2018. Correction scheme for point-particle models applied to a nonlinear drag law in simulations of particle-fluid interaction. Int. J. Multiphase Flow https://doi.org/10.1016/j.ijmultiphaseflow.2018.01.003.

Huang, F., Kang, Y., You, Z., You, L., Xu, C., 2017. Critical Conditions for Massive Fines Detachment Induced by Single-Phase Flow in Coalbed Methane Reservoirs: Modeling and Experiments. Energy & Fuels 2017 31 (7), 6782–6793. https://doi.org/10.1021/acs.energyfuels.7b00623.

Joodat, S.H.S., Nakshatrala, K.B., Ballarini, R, 2018. Modeling flow in porous media with double porosity/permeability: A stabilized mixed formulation, error analysis, and numerical solutions. Comp. Method Appl. Mech. Eng. 3371, 632–676. https://doi.org/10.1016/j.cma.2018.04.004.

Ju, B., Yang, Y., Brantson, T., Chi, J., 2017. A numerical simulator developed for modeling permeability control for enhanced oil recovery. J. Petrol. Sci. Eng..

Kapellos, G.E., Alexiou, T.S., Payatakes, A.C., 2007. Hierarchical simulator of biofilm growth and dynamics in granular porous materials. Adv. Water Resour. 30 (6–7), 1648–1667. https://doi.org/10.1016/j.advwatres.2006.05.030.

Klimenko, L.S., Maryshev, B.S., 2019. Numerical simulation of micro channel blockage by the random walk method. Chem. Eng. J. https://doi.org/10.1016/j.cej.2019.122644.

Koivu, V., Decain, M., Geindreau, C., Mattila, K., Bloch, J.-F., Kataja, M., 2009. Transport properties of heterogeneous materials. Combining computerized X-ray micro-tomography and direct numerical simulations. Int. J. Comput. Fluid Dyn. 23, 713–721.

Koponen, A., Kandhai, D., Hellén, E., Alava, M., Hoekstra, A., Kataja, M., Niskanen, K., Sloot, P., Timonen, J., 1998. Permeability of three-dimensional random fiber webs. Phys. Rev. Lett. 80, 716–719.

Kozeny, J., 1927. ÜberkapillareLeitung des WassersimBoden. SitzungsberAkadWiss Wien 136 (2a), 271306.
Lee, S.L., Yang, J.H., 1997. Modelling of Darcy-Forchheimer drag for fluid flow across a bank of circular cylinders. Int. J. Heat Mass Transf. 40 (13), 3149–3155.
Li, Q., Prigiobbe, V., 2018. Numerical Simulations of the Migration of Fine Particles through Porous Media. Transport in Porous Media 122, 745–759. https://doi.org/10.1007/s11242-018-1024-3.
Li, T., Li, S., Zhao, J., Lu, P., Meng, L., 2012. Sphericities of non-spherical objects. Particuology 10 (1), 97–104. https://doi.org/10.1016/j.partic.2011.07.005.
Liu, M., Mostaghimi, P., 2017. High-resolution pore-scale simulation of dissolution in porous media. Chem. Eng. Sci. 161, 360–369.
Liu, M., Starchenko, V., Anovitz, L.M., Stack, A.G., 2020. Grain detachment and transport clogging during mineral dissolution in carbonate rocks with permeable grain boundaries. GeochimicaetCosmochimicaActa 280, 202–220.
Lima, M.C.O., Pontedeiro, E.M., Ramirez, M., Boyd, A., Th van Genuchten, M., Borghi, L., Couto, P., Raoof, A., 2020. Petrophysical Correlations for the Permeability of Coquinas (Carbonate Rocks). Transport in Porous Media 1–22. https://doi.org/10.1007/s11242-020-01474-1.
Mattila, K., Puurtinen, T., Hyväluoma, J., Surmas, R., Myllys, M., Turpeinen, T., Robertsen, F., Westerholm, J., Timonen, J., 2016. A prospect for computing in porous materials research: very large fluid flow simulations. J. Comp. Syst. Sci. 12, 62–76.
Montessori, A., Prestininzi, P., La Rocca, M., Falcucci, G., Succi, S., Kaxiras, E., 2016. Effects of Knudsen diffusivity on the effective reactivity of nanoporous catalyst media. J. Comput. Sci. 17, 377–383. doi.org/10.1016/j.jocs.2016.04.006.
Montessori, A., Prestininzi, P., La Rocca, M., Succi, S., 2015. Lattice Boltzmann approach for complex nonequilibrium flows. Phys. Rev. E 92 (4), 043308. https://doi.org/10.1103/PhysRevE.92.043308.
Netter, P., Conti, C. (2016). Efficiency of industrial filters for molten metal treatment evaluation of a filtration process model. *Essential Readings in Light Metals*. 271-284. doi:10.1007/978-3-319-48228-6_33.
Parvan, A., Jafari, S., Rahnama, M., Apourvari, S.N., Raoof, A., 2020. Insight into Particle retention and clogging in porous media; a pore scale study using Lattice Boltzmann Method. Adv. Water Resour., 103530 https://doi.org/10.1016/j.advwatres.2020.103530.
Parvan, A., Rahnama, M., Jafari, S., JahanshahiJavaran, E., 2019. Evaluation of force term in lattice Boltzmann method with discrete external boundary force for flow over an immersed body. Particul. Sci. Tech. 1–14. https://doi.org/10.1080/02726351.2018.1491486.
Pham, N.H., Voronov, R.S., Tummala, N.R., Papavassiliuo, D.V., 2014. Bulk stress distributions in the pore space of sphere-packed beds under Darcy-flow conditions. Phys. Rev. E 89, 033016.
Porter, B., Zauel, R., Stockman, H., Guldberg, R., Fyhrie, D., 2005. 3-D computational modeling of media flow through scaffolds in a perfusion bioreactor. J. Biomech.38 (3) 543–549.
Qiu, Q., 2015. Univer. Delaware (PhD thesis).
Rabbani, H.S., Zhao, B., Juanes, R., Shokri, N., 2018. Pore geometry control of apparent wetting in porous media. Sci. Rep. 8 (1). https://doi.org/10.1038/s41598-018-34146-8.
Raoof, A., Hassanizadeh, S.M., 2010. A New Method for Generating Pore-Network Models of Porous Media. Transp Porous Med 81, 391–407. https://doi.org/10.1007/s11242-009-9412-3.
Raoof, A., Hassanizadeh, S. M., Leijnse, A. (2010). Up scaling Transport of Adsorbing Solutes in Porous Media: Pore-Network Modelling. Volume9, Issue3pp.624-636. doi:10.2136/vzj2010.0026.
Raoof, A.; Nick, H.M.; Hassanizadeh, S.M.; Spiers, C.J. (2013). *Computers and Geosciences*, volume 61, pp. 160–174. doi:10.1016/j.cageo.2013.08.005.
Rueden, C.T., Schindelin, J., Hiner, M.C., et al., 2017. ImageJ2: imageJ for the next generation of scientific image data. BMC Bioinformat 18, 529. doi.org/10.1186/s12859-017-1934-z. PMID 29187165.
Schulz, R., Knabner, P., 2016. Derivation and analysis of an effective model for biofilm growth in evolving porous media. Math. Method Appl. Sci. 40 (8), 2930–2948. https://doi.org/10.1002/mma.4211.
Silliman, S.E., Dunlap, R., Fletcher, M, Schneegurt, M.A., 2001. Bacterial transport in heterogeneous porous media: Observations from laboratory experiments. Water Resour. Res. 37, 2699–2707.
Stewart, M.P., Buriak, J.M., (2000). Chemical and Biological Applications of Porous Silicon Technology. 12, 12, 859-869. doi:10.1002/1521-4095(200006)12:12≤859::AID-ADMA859≥3.0.CO;2-0.
Stokes, G.G., 1850. On the effect of the inertial friction of fluids on the motion of pendulums. Trans. Camb. Phil. Soc. IX, 8.
Succi, S., 2001. The Lattice Boltzmann Equation for Fluid Dynamics and Beyond. Clarendon Press, Oxford.
Sukop, M.C., Thorne Jr., D.T., 2006. Lattice Boltzmann Modeling: An Introduction for Geoscientists and Engineers. Springer, Berlin.
Thullner, M., 2010. Comparison of bioclogging effects in saturated porous media within one- and two-dimensional flow systems. Ecol. Eng. 36 (2), 176196. https://doi.org/10.1016/j.ecoleng.2008.12.037.
Tong, D., Zhuang, J., Chen, X., 2019. Reactive Transport and Removal of Nutrients and Pesticides in Engineered Porous Media. Water 11 (7), 1316. https://doi.org/10.3390/w11071316.
Tufenkji, N., 2007. Modeling microbial transport in porous media: Traditional approaches and recent developments. Adv. Water Resour. 30 (6–7), 1455–1469. https://doi.org/10.1016/j.advwatres.2006.05.014.
Verma, A., Pruess, K., 1988. Thermohydrological conditions and silica redistribution near high-level nuclear wastes emplaced in saturated geological formations. J. Geophys. Res. Solid Earth 93 (B2), 11591173. https://doi.org/10.1029/JB093iB02p01159.
Voronov, R., VanGordon, S., Sikavitsas, V.I., Papavassiliou, D.V., 2010. Computational modeling of flow-induced shear stresses within 3D salt-leached porous scaffolds imaged via micro-CT. J. Biomech. 43, 1279–1286. https://doi.org/10.1016/j.jbiomech.2010.01.007.
Wang, H., Xin, J., Zheng, X., Li, M., Fang, Y., Zheng, T., 2020. Clogging evolution in porous media under the coexistence of suspended particles and bacteria: Insights into the mechanisms and implications for groundwater recharge. J. Hydrol. 582, 124554. https://doi.org/10.1016/j.jhydrol.2020.124554.
Xiao, F., Yin, X., 2016. Geometry models of porous media based on Voronoi tessellations and their porosity–permeability relations. Comp. Math. Appl. 72 (2), 328–348. https://doi.org/10.1016/j.camwa.2015.09.009.
Yazdchi, K., Srivastava, S., Luding, S., 2011. Microstructural effects on the permeability of periodic fibrous porous media. Int. J. Multiphase Flow 37 (8), 956–966. https://doi.org/10.1016/j.ijmultiphaseflow.2011.05.003.
Yoon, H., Kang, Q., Valocchi, A.J., 2015. Lattice Boltzmann-Based Approaches for Pore-Scale Reactive Transport. Rev. Mineral. Geochem. 80 (1), 393–431. https://doi.org/10.2138/rmg.2015.80.12.
Zhang, L., Soong, Y., Dilmore, R., Lopano, C., 2015. Numerical simulation of porosity and permeability evolution of Mount Simon sandstone under geological carbon sequestration conditions. Chem. Geol. 403, 112. https://doi.org/10.1016/j.chemgeo.2015.03.014.
Zhang, D., Zabarankinb, M., Prigiobbe, V., 2019. Modeling salinity-dependent transport of viruses in porous media. Adv. Water Resour. 127, 252–263. https://doi.org/10.1016/j.advwatres.2019.03.017.
Zheng, X.L., Shan, B.B., Chen, L., Sun, Y.W., Zhang, S.H., 2014. Attachment–detachment dynamics of suspended particle in porous media: Experiment and modeling. J. Hydrol. 511, 199–204. https://doi.org/10.1007/s11242-011-9839-1.
Zhou, Z., Du, X., Wang, S., Zang, H., 2018. Analysis and engineering application investigation of multiple-hole grouting injections into porous media considering filtration effects. Construct. Build. Mater. 186, 871–883. https://doi.org/10.1016/j.conbuildmat.2018.08.005.